Thermal Decomposition of Trimethylgallium $Ga(CH_3)_3$: A Shock-Tube Study and First-Principles Calculations

Mustapha Fikri,*,† Alexander Makeich,†,‡ Georg Rollmann,§ Christof Schulz,†,|| and Peter Entel§

IVG, Theoretische Physik, and CeNIDE, Center for Nanointegration, Universität Duisburg-Essen, D-47048, Duisburg, Germany

Received: February 20, 2008; Revised Manuscript Received: April 16, 2008

The thermal decomposition of $Ga(CH_3)_3$ has been studied both experimentally in shock-heated gases and theoretically within an ab-initio framework. Experiments for pressures ranging from 0.3 to 4 bar were performed in a shock tube equipped with atomic resonance absorption spectroscopy (ARAS) for Ga atoms at 403.3 nm. Time-resolved measurements of Ga atom concentrations were conducted behind incident waves as well as behind reflected shock waves at temperatures between 1210 and 1630 K. The temporal variation in Ga-atom concentration was described by a reaction mechanism involving the successive abstraction of methyl radicals from $Ga(CH_3)_3$ (R1), $Ga(CH_3)_2$ (R2), and $GaCH_3$ (R3), respectively, where the last reaction is the rate-limiting step leading to Ga-atom formation. The rate constant of this reaction (R3) was deduced from a simulation of the measured Ga-atom concentration profiles using thermochemical data from ab-initio calculations for the reactions R1 and R2 as input. The Rice−Ramsperger−Kassel−Marcus (RRKM) method including variational transition state theory was applied for reaction R3 assuming a loose transition state. Structural parameters and vibrational frequencies of the reactant and transition state required for the RRKM calculations were obtained from first-principles simulations. The energy barrier E_3^0 of reaction R3, which is the most sensitive parameter in the calculation, was adjusted until the RRKM rate constant matched the experimental one and was found to be $E_3^0 = 288$ kJ/mol. This value is in a good agreement with the corresponding ab-initio value of 266 kJ/mol. The rate constant of reaction R3 was found to be $k_3/(\mathrm{cm}^3\ \mathrm{mol}^{-1}\ \mathrm{s}^{-1}) = 2.34 \times 10^{11} \exp[-23330(\mathrm{K}/T)]$.

I. Introduction

Gallium nitride (GaN) and monoclinic gallium oxide (β-Ga_2O_3) possess the widest band gaps among semiconducting materials that exhibit luminescence and are therefore potential candidates for applications in optoelectronic devices[1–3] as well as high-temperature gas sensors.[4] When thin films with uniform thickness of fine particles are needed, GaN and Ga_2O_3 are often produced in high-temperature gas-phase processes, e.g., chemical vapor deposition (CVD), high-temperature flow reactors, and flames.[5] Here, trimethylgallium $Ga(CH_3)_3$ has recently become the most commonly used precursor material. For well-controlled gas-phase synthesis, precise knowledge of the kinetics of the elementary gas-phase reactions is required. In our institute, the gas-phase reactions of some metal chlorides were previously studied.[6–9] This series is now continued by the thermal decomposition of $Ga(CH_3)_3$.

Pioneering work on the thermal decomposition of trimethylgallium was carried out by Jacko and Price,[10] who postulated a mechanism described by a successive homolytic cleavage of the Ga−C bond. The reactions involved are, therefore,

$$Ga(CH_3)_3 \rightarrow Ga(CH_3)_2 + CH_3 \qquad (R1)$$

$$Ga(CH_3)_2 \rightarrow GaCH_3 + CH_3 \qquad (R2)$$

$$GaCH_3\,(+M) \rightarrow Ga + CH_3\,(+M) \qquad (R3)$$

It should be noted, however, that the third methyl radical was not cleaved during their experiments. The energy barrier $E_3^0 =$ 324 kJ/mol for reaction R3 was determined by assuming that the activation energies for reactions R1 and R2 approximately equal the respective bond strengths. A slight pressure dependence was found for the rate constants below 30 mbar. In an effort to determine the rate constant of the thermal decomposition of $Ga(CH_3)_3$, DenBaars et al.[11] studied the decomposition kinetics of trimethylgallium in a H_2 flow by infrared−absorption spectroscopy. They obtained a lower activation energy $E_{a,3} =$ 240−260 kJ/mol than Jacko and Price, assuming a homogeneous unimolecular process for the decomposition of $Ga(CH_3)_3$. This activation energy was interpreted as an approximate dissociative bond energy, E_1^0, for the first methyl group of $Ga(CH_3)_3$. In contrast to the work of Jacko and Price, three methane molecules for each $Ga(CH_3)_3$ molecule were observed at higher temperatures, implying the cleavage of the methyl radical from $GaCH_3$. These findings are at odds with the assumption that the third step is heterogeneous, especially since there is evidence that $GaCH_3$ tends to react on the substrate surface.[10,12] By applying atomic resonance absorption spectroscopy, Haigh and O'Brien[12] could not detect Ga atoms and concluded that the pyrolysis of $GaCH_3$ does not proceed in the gas phase toward producing Ga atoms. Shock-tube studies are, however, not affected by this process.

There are also controversies concerning the effect of the carrier gas on the reaction rate.[13–15] In an effort to assess the role of the carrier gas on the decomposition rate of $Ga(CH_3)_3$, Larsen et al.[16] studied the effect of carrier gases such as He

* To whom correspondence should be addressed. Telephone: +49(0)203-379-3037. Fax: +49(0)203-379-3087. E-mail: mustapha.fikri@uni-due.de.
† IVG.
‡ Current address: Institute for High Energy Density, Russian Academy of Sciences, Moscow, Russia.
§ Theoretische Physik.
|| CeNIDE.

10.1021/jp801516y CCC: $40.75
Published on Web 06/25/2008

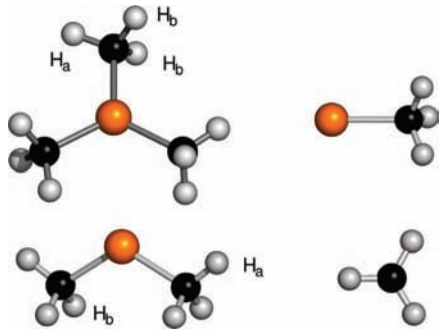

Figure 1. Optimized geometries of the different molecular species involved in the thermal decomposition of $Ga(CH_3)_3$.

and N_2 and scavengers such as toluene. They concluded that toluene acts as an inhibitor and prevents further reaction of the CH_3 groups. In He or N_2 atmosphere, however, the methyl groups interact with the parent molecule leading to CH_4.

Several groups have performed first-principles simulations in order to investigate the elementary processes involved in the thermal decomposition of $Ga(CH_3)_3$. In an early study, Oikawa et al.[17] calculated the rate constant of reaction R1 within the framework of the Hartree−Fock (HF) approximation. The critical bond length of the dissociating Ga−C bond in the transition state was determined to be 4.39 Å using the method proposed by Hase.[18] The resulting rate constant of $k(T)/s^{-1} = 10^{16.33}\exp[-(260/(kJ/mol))/2.303RT]$ roughly reproduces the experimental value of Jacko and Price.[10] The Ga−C bond strengths in $Ga(CH_3)_3$, $Ga(CH_3)_2$, and $GaCH_3$ were computed by Edwards and Jones[19] within HF as well as second-order perturbation theory to account for correlation effects. The authors obtained, in agreement with the experimental findings, the weakest bond in $Ga(CH_3)_2$. In addition, also in agreement with the estimate of Jacko et al., they found the bond in $GaCH_3$ being significantly stronger (HF, 96 kJ/mol; MP2, 46 kJ/mol) than in $Ga(CH_3)_3$. In contrast to that, from a detailed analysis using a variety of different ab-initio methods, Trachtman et al. found the Ga−C bond to be the strongest in $Ga(CH_3)_3$, followed by $GaCH_3$ and $Ga(CH_3)_2$.[20] However, in all three studies it remains unclear to some extent whether the results can be considered converged with respect to the size of the one-electron basis. More recent investigations have mainly been concerned with the parent molecule, $Ga(CH_3)_3$, and the first decomposition step: By employing several ab-initio schemes including density functional theory (DFT), Maung[21] and Pelekh and Carr[22] report equilibrium structures and energies of $Ga(CH_3)_3$, while Jensen[23] has computed the vibrational spectrum and found reasonable agreement with corresponding experimental data. Schmid and Basting have investigated the kinetics of reaction R1 within variational transition-state theory;[24] ground-state geometries of the species involved in reactions R1–R3 calculated within a hybrid-DFT method have recently been presented as part of more general surveys.[25,26]

The present study sheds light onto the kinetics of the thermal decomposition of $Ga(CH_3)_3$, which is regarded as an important route toward the synthesis of gallium-containing materials such as Ga_2O_3 and GaN, but has been discussed controversially in the literature. In a separate paper, the results of this study were taken into account to study the high-temperature kinetics of the reaction of Ga atoms with NH_3.[27]

The best description of the Ga-concentration profiles obtained in the thermal decomposition of $Ga(CH_3)_3$ in shock-tube experiments by means of atomic resonance absorption spectroscopy (ARAS) was achieved by fitting the profiles using values for the energy barriers of reactions R1 and R2 calculated from first principles. This procedure yields the rate constant of reaction R3, which turns out to be the rate-limiting step. Preexponential factors for the reactions R1 and R3 were taken from similar reactions. Furthermore, the *T*- and the *p*-dependencies of the rate constant k_3 were well-described with the Rice−Ramsberger−Kassel−Marcus (RRKM) method by using ab-initio data for the geometries of $GaCH_3$ in the ground and the transition states. The fitting parameter from the calculation was the energy barrier E_3^0, which is in good agreement with the corresponding ab-initio value.

In the following section, we describe details of the ab-initio calculations and present results for the molecules involved in reactions R1–R3, in particular the strengths of the dissociating Ga−C bonds. Afterwards, the experimental setup is presented, and the results of the Ga-atom concentration profile measurements as well as the kinetic modelling is discussed. Results of the RRKM simulations for reaction R3 are presented in section IV, followed by concluding remarks in the last section.

II. Ab Initio Simulations

Computational Method. We have optimized the geometries of the species involved in the thermal decomposition of $Ga(CH_3)_3$ in the framework of spin-polarized DFT using plane waves as basis functions as well as several localized basis sets. In all calculations, we have neglected relativistic effects, which are considered to only have a small influence on the geometries, and a negligible effect on the energetics. For the relaxed structures, harmonic vibrational frequencies were computed in order to verify that they form true minima on the respective potential-energy surface.

The plane-wave calculations were performed both by treating the Ga 3d electrons as core states and by explicitly including them in the valence shell. For the C atoms, the 2s and 2p electrons were treated as valence states. The remaining electrons together with the nuclei were described by the projector-augmented wave (PAW)[28] method as implemented in the Vienna ab-Initio Simulation Package (VASP).[29,30] The cut-off energy for the basis set was kept fixed at 500 eV, and all systems were placed in cubic supercells of 15 Å length, which proved to be sufficient to ensure that the interaction between the considered molecule and its periodic images is negligible. Exchange and correlation were described by the functional proposed by Perdew, Burke, and Ernzerhof,[31] denoted as PBE.

These simulations using localized basis sets of different size (the largest being the aug-cc-pVQZ basis of quadruple-ζ quality) were carried out with the Gaussian03 program package.[32] For the numerical integrations, the "ultrafine" grid was used throughout, which includes 99 radial shells and 590 angular points per shell. In addition to the PBE functional, the hybrid B3LYP method was employed, which consists of the three-parameter exchange functional proposed by Becke,[33] where part of the DFT exchange energy is replaced by the corresponding HF term and the correlation functional of Lee, Yang, and Parr.[34]

To obtain a measure for the uncertainty inherent to the DFT calculations, we have investigated the different molecular species also within coupled cluster theory with single and double excitations (CCSD).[35] However, while we could treat $GaCH_3$ as well as the CH_3 radical using a large quadruple-ζ basis, we were limited to considerably smaller basis sets in the case of $Ga(CH_3)_2$ and $Ga(CH_3)_3$ due to the high computational demands of that method.

Results of ab-Initio Simulations. The ground-state structures obtained for the relaxed species did not depend on the employed

TABLE 1: Optimized Values of Selected Interatomic Distances (Å) in the Relaxed Species, Obtained with Different Combinations of ab Initio Methods and Basis Sets[a]

	$Ga(CH_3)_3$			$Ga(CH_3)_2$			$GaCH_3$		
	Ga−C	C−H_a	C−H_b	Ga−C	C−H_a	C−H_b	Ga−C	C−H	CH_3C−H
PBE/PAW, 3e⁻	1.999	1.097	1.100	2.030	1.095	1.101	2.066	1.103	1.087
PAW, 13e⁻	1.978	1.098	1.101	2.010	1.095	1.101	2.049	1.103	
PBE/6-31+G(d)	1.983	1.103	1.106	2.000	1.101	1.107	2.023	1.109	1.091
aug-cc-pVTZ	1.989	1.097	1.101	2.015	1.095	1.101	2.051	1.103	1.086
aug-cc-pVQZ	1.986	1.097	1.100	2.012	1.095	1.101	2.047	1.103	1.086
B3LYP/6-31+G(d)	1.984	1.095	1.099	2.004	1.093	1.099	2.025	1.101	1.083
aug-cc-pVTZ	1.991	1.089	1.092	2.020	1.087	1.093	2.054	1.095	1.078
aug-cc-pVQZ	1.988	1.089	1.092	2.017	1.087	1.092	2.050	1.094	1.077
CCSD/6-31+G(d)	1.995	1.098	1.100	2.083	1.095	1.101	2.028	1.102	1.084
cc-pVTZ	—	—	—	1.990	1.087	1.093	2.023	1.095	1.078
aug-cc-pVTZ	—	—	—	—	—	—	2.018	1.095	1.078
cc-pVQZ	—	—	—	—	—	—	2.011	1.094	1.078
experiment	1.967	1.082	1.082						

[a] Experimental values from ref 36 are added for comparison. For the definition of H_a and H_b, see Figure 1.

TABLE 2: Zero-Point Corrected Bond Strengths E^0 (kJ/mol) of $Ga(CH_3)_3$, $Ga(CH_3)_2$, and $GaCH_3$

	$(CH_3)_2Ga-CH_3$	CH_3Ga-CH_3	CH_3-Ga
PBE/PAW, 3e⁻	324	151	256
PAW, 13e⁻	329	153	258
PBE/6-31+G(d)	320	168	289
aug-cc-pVTZ	300	145	266
aug-cc-pVQZ	301	145	266
B3LYP/6-31+G(d)	305	141	270
aug-cc-pVTZ	285	119	247
aug-cc-pVQZ	286	119	247
CCSD/6-31+G(d)	315	135	247
cc-pVTZ	—	138	257
aug-cc-pVTZ	—	—	270
cc-pVQZ	—	—	260

computational scheme. In particular, the molecular symmetry is C_{3h} for $Ga(CH_3)_3$, C_{2v} for $Ga(CH_3)_2$, and C_{3v} for $GaCH_3$ and CH_3, which is in agreement with results from previous studies (for a discussion on the effect of the nearly free-rotating methyl groups, see ref 19). The corresponding arrangements of the atoms are depicted in Figure 1. For $Ga(CH_3)_3$ and $Ga(CH_3)_2$, there are two different kinds of hydrogen atoms, which are not equivalent by symmetry: While the atoms denoted as H_a lie in the plane spanned by the Ga and C atoms, the H_b atoms do not, resulting in slightly different bond lengths and angles.

Optimized values for characteristic interatomic distances are compiled in Table 1. It is observed that the C−H bond lengths are affected only slightly by the chosen level of theory, with differences below 0.02 Å. In contrast to that, the calculated Ga−C distances are subject to considerably larger variation. Here, best agreement with the experimental value[36] for $Ga(CH_3)_3$ is obtained by the PBE/PAW calculations and a plane-wave basis set. However, explicitly treating the Ga 3d electrons as valence states is clearly necessary in order to get converged values. Corresponding results are then very similar to the all-electron PBE data obtained with localized basis sets. With respect to the latter, no significant differences (<0.003 Å) are observed between values computed by using a triple-ζ and a quadruple-ζ basis, so we consider the aug-cc-pVQZ results to be sufficiently converged. The Ga−C distances obtained with the 6-31+G(d) basis are systematically smaller and may be taken as a measure for the incompleteness of that basis. For all species, the C−H distances obtained from the B3LYP approach are smaller than the PBE values and are, in the case of $GaCH_3$, closer to the experimental data.[36] At the same time, however, the Ga−C bond lengths are slightly increased.

With respect to the CCSD calculations, we note that a double-ζ basis is not sufficient to describe the geometries of the Ga-containing species accurately. This becomes especially evident in the case of the $Ga(CH_3)_2$ molecule, where a huge drop of nearly 0.1 Å in Ga−C distance occurs when changing from 6-31G+ to cc-pVTZ. For $GaCH_3$, where we were able to perform calculations with substantially larger basis sets, there is still some variation in the Ga−C bond length even at the cc-pVQZ level. However, as this variation is likely to be present also for the larger species, it seems reasonable to assume that associated errors cancel (at least in part) when relative energies, i.e., bond strengths, are computed. When we compare the DFT results for $GaCH_3$ with the outcome of the corresponding CCSD calculations, we note that there are considerable discrepancies especially in the Ga−C distances, the PBE and B3LYP bond lengths being substantially larger. Nevertheless, the same argument as above leads to the conjecture that calculated energy differences will be considerably more accurate.

This is indeed the case, as the bond strengths of $Ga(CH_3)_3$, $Ga(CH_3)_2$, and $GaCH_3$ calculated as total energy differences (including zero-point corrections) between reactants and products of reactions R1–R3 listed in Table 2. In all cases, the Ga−C bond is strongest in $Ga(CH_3)_3$, followed by $GaCH_3$ and $Ga(CH_3)_2$. This agrees well with the findings of Trachtman et al.[20] but is in contrast to the results of Edwards and Jones,[19] who obtained the opposite order for the bond strength in $Ga(CH_3)_3$ and $GaCH_3$, maybe due to insufficiencies in their computational scheme.

When comparing the CCSD results for $GaCH_3$, one observes that all values are very similar. The addition of diffuse functions to the cc-pVTZ basis slightly increases the energy barrier, which is again lowered when the size of the basis set is further increased to quadruple-ζ quality. Nevertheless, even the 6-31+G value is not off by too much. In addition, also the two values computed for $Ga(CH_3)_2$ are nearly identical, despite the pronounced differences in the underlying geometries. Among the DFT results, the PBE functional seems to perform best, while B3LYP yields bond strengths that are slightly too small. The PBE/aug-cc-pVQZ value for $GaCH_3$ of 266 kJ/mol is only 6 kJ/mol larger than the CCSD benchmark value—a difference that will presumably even be reduced when further increasing the basis in the CCSD calculation by adding diffuse functions to the quadruple-ζ basis. Therefore, we have opted to use the PBE/aug-cc-pVQZ results of the energy barriers, structures, and vibratin frequencies as input for the modeling of the experi-

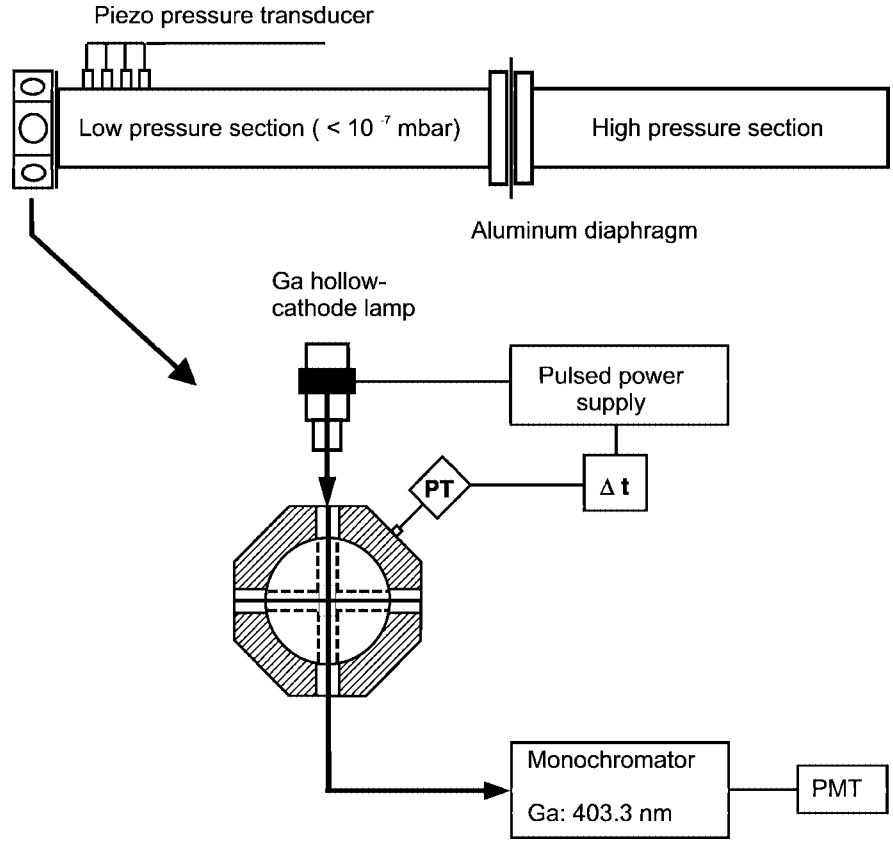

Figure 2. Experimental setup.

TABLE 3: Experimental Conditions

experiment sets	$x(Ga(CH_3)_3)$ in Ar/ppm	T/K	total density/ (10^{-6} mol cm^{-3})
1	6−40	1330−1570	2.0−2.8
2	1−10	1210−1600	14.9−17.9
3	8	1368−1630	19.0−30.6

mentally measured Ga-atom concentration profiles as well as the RRKM calculations.

III. Experimental Section

The experiments were carried out in a conventional stainless-steel pressure-driven diaphragm shock tube with an internal diameter of 80 mm. It is divided by a thin aluminum diaphragm into a driver section of 3.5 m and a driven section of 5.7 m in length. The internal surface has been honed and electropolished for ultrahigh-vacuum (UHV) purposes. The driven section was pumped down to pressures below 2×10^{-8} mbar by a turbo molecular pump. Gas mixtures were prepared manometrically in a stainless steel UHV storage cylinder, which also was evacuated using a separate turbo molecular pumping unit. The shock speed was measured over three intervals using four piezoelectric pressure gauges (PCB 113A27). The data were recorded with a time resolution of 100 ns. The temperature and pressure behind the reflected shock wave were computed from the measured incident shock speed and the speed attenuation using a one-dimensional shock model (shock tube code of the CHEMKIN Package[37]). The estimated uncertainty in reflected shock temperature is less than ±15 K in the temperature and time range of our measurements. The experimental setup used is depicted in Figure 2.

Concentrations of ground-state $Ga(^2P^0_{1/2})$ atoms were monitored by time-resolved atomic resonance absorption spectroscopy (ARAS). A gallium hollow-cathode lamp (Heraeus) operated by a pulsed (5 ms) power source, a 0.25 m Jarrel-Ash monochromator, and a UV−vis photomultiplier (Hamamatsu Photonics 1P28) were arranged to measure light attenuation by Ga atoms at $\lambda = 403.299$ nm at a position of 10 mm upstream of the end wall. For the quantitative determination of the Ga-atom concentrations, the ARAS technique requires calibration due to the unknown spectral profiles of these absorption lines. Therefore, a series of shock-wave experiments with known concentrations of $Ga(CH_3)_3$ (1−10 ppm) were performed at temperatures above 1200 K with typical fractional absorptions A_λ ranging from 0.2 to 0.8. At these conditions, the Ga-atom concentration is equal to the initial $Ga(CH_3)_3$ concentration. It is reached after reaction times of a few microseconds. The result of the calibration can be interpreted with the Beer−Lambert law:

$$A_{Ga} = 1 - \exp(-l\sigma_{403.29}[Ga])$$

where $l = 7.9$ cm is the absorption path length. The atom absorption cross-section was $\sigma_{403.299} = 2.93 \times 10^{-15}$ cm^2. A temperature dependence of the calibration was not found in the 1290−2320 K range.

The kinetic experiments were performed in the present study at 0.3, 1.7, and 3.4 bar at various temperatures following the variation of the gallium concentration by ARAS. The experiments at 0.3 bar were performed behind incident waves. The purpose of this set of experiments was the determination of the pressure dependence of the rate constants of reaction R3.

Test gas mixtures of $Ga(CH_3)_3$ highly diluted in argon (2−10 ppm) were prepared manometrically in a stainless-steel storage cylinder. Argon used in the present study was of the highest commercially available purity (≥99.9999%). $Ga(CH_3)_3$ is liquid at room temperature and is specified with a purity better than 99.5%.

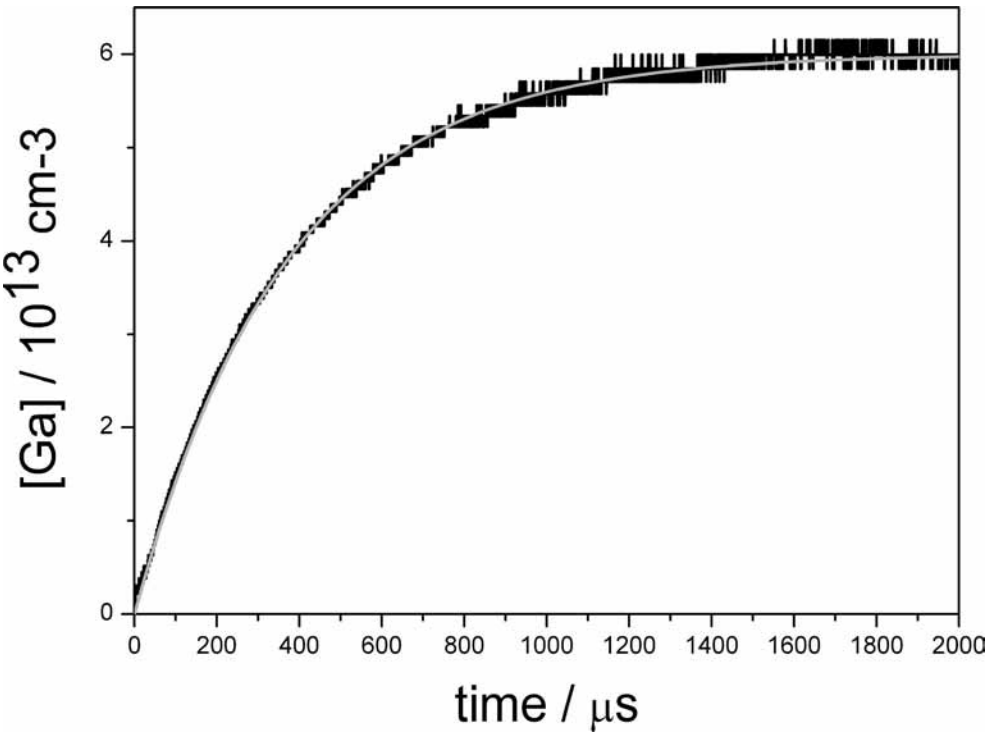

Figure 3. Typical measured concentration profiles of Ga atoms in a $Ga(CH_3)_3$−Ar mixture shock-heated to a temperature of 1465 K at pressure of 1.79 bar. The gray line denotes the simulation based on the simplified reaction model consisting of reactions R1–R3 in Table 4.

TABLE 4: Reaction Mechanism for the Thermal Decomposition of Trimethylgallium

reactions	$k = A \exp(E_a/RT)$ A /s^{-1}	E_a/R
$Ga(CH_3)_3 \rightarrow Ga(CH_3)_2 + CH_3$	$10^{15.6}$	36464
$Ga(CH_3)_2 \rightarrow GaCH_3 + CH_3$	$10^{15.4}$	17474
$GaCH_3 + M \rightarrow Ga + CH_3 + M$		adjusted (see text)

There was an experimental difficulty that a small amount of $Ga(CH_3)_3$ disappeared due to adsorption on the surface of the stainless-steel storage vessel. Therefore, it was necessary to correct the initial $Ga(CH_3)_3$ concentration from the steady-state Ga-atom concentration obtained by ARAS. The corrected values were taken to simulate the Ga-atom concentration profiles with the CHEMKIN package.

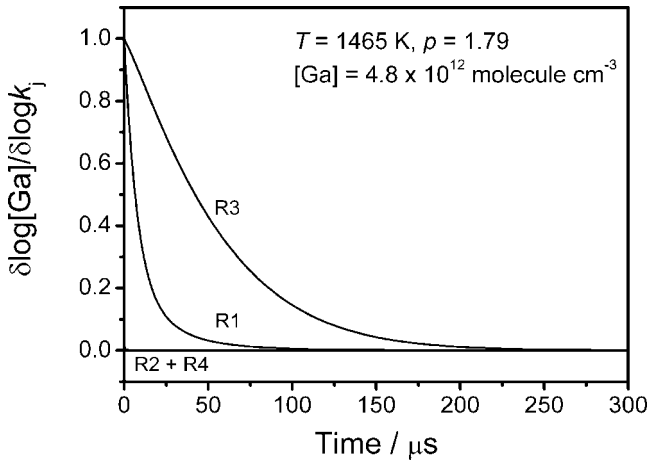

Figure 4. Normalized sensitivity analysis of rate coefficients for Ga-atom formation at 1465 K and 1.79 bar for $Ga(CH_3)_3 \rightarrow Ga(CH_3)_2 + CH_3$ (R1), $Ga(CH_3)_2 \rightarrow Ga(CH_3) + CH_3$ (R2), and $GaCH_3 + M \rightarrow Ga + CH_3 + M$ (R3).

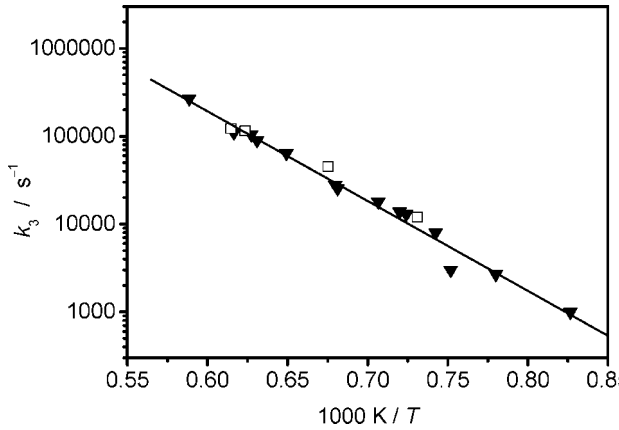

Figure 5. Arrhenius plot of the first-order rate constant for reaction R3 using the data of 1.7 (triangles) and 3.4 bar (squares). The solid line shows the least-squares fit of the experimental data.

IV. Results and Discussion

Table 3 shows an overview of the experimental conditions of the measurements conducted in this study.

In a first series, Ga-atom concentration profiles were measured behind reflected waves in mixtures containing $Ga(CH_3)_3$ highly diluted in argon to avoid secondary reactions (experimental numbers 1 and 2). The second series (Table 3, number 3) of experiments was carried out behind incident waves to check the pressure dependence of reaction R3. Figure 3 shows the temporal variation of the Ga-atom concentrations at $T = 1465$ K and a pressure of $p = 1.79$ bar. At the arrival of the shock wave ($t = 0$) the signal rises rapidly and reaches the steady-state concentration after 1 ms. The Ga-atom concentration remained constant showing that consumption reactions with respect to Ga atoms do not play a significant role on the time scale of our experiments. At lower temperatures, the Ga-atom concentration increases more slowly showing an induction time of a few microseconds.

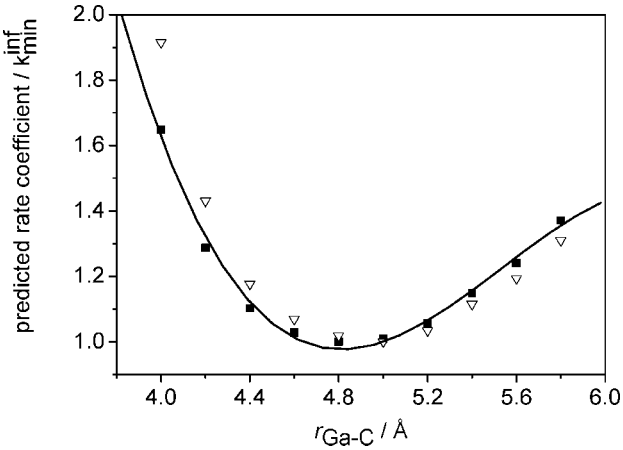

Figure 6. Variations of the RRKM high-pressure limit rate coefficients for reaction R3 normalized to k_{min}^{∞} as a function of the distance Ga−C bond being cleaved. Squares, $T = 1500$ K; triangles, $T = 1300$ K.

A sensitivity analysis of the same experiment of Figure 3 was performed for the reactions R1–R3 as well as for reaction R4 of Ga atoms with the parent molecule $Ga(CH_3)_3$.[38] For this purpose, CHEMKIN[37] and SENKIN[39] program codes were utilized to identify the rate-limiting steps in the production of Ga atoms. From Figure 4, it can be seen clearly that the Ga-atom formation is insensitive to reactions R1 and R4. Reaction R2 has a slight sensitivity at earlier times and could not be measured in this study. Reactions R1 and R2 have no significant influence. Therefore, reaction R3, which is the rate-determining reaction step, was directly linked to the production of Ga atoms. Additionally, it was not possible to fit the Ga-atom concentration profiles at low as well as at high temperature by a global mechanism assuming one-step reaction. Simulations with the mechanism suggested by Jacko and Price[10] resulted in reaction rates that are too slow and could not reproduce the experimental data.

To simulate the Ga-atom concentration time profiles, we adopted a simplified mechanism by evaluating the rate constants of reactions R1 and R2, keeping them constant, and fitting only the last reaction step (R3). For the activation energies $E_{a,1}$ and $E_{a,2}$, the PBE/aug-cc-pVQZ values for E^0 (see Table 2) of 301 and 145 kJ/mol, respectively, were taken into account. The preexponential A-factors, which are typically very high for loose transition cases, were adopted from A-factors for similar reaction types. Table 4 summarizes the simplified mechanism used in this study.

Following this strategy, the Ga-concentration profiles were well-reproduced by the simulation and the rate constant k_3 was evaluated. The Arrhenius plot obtained by this method is shown in Figure 5. Because the results for the rate constants were constant within the experimental errors when increasing the pressure from 1.3 to 3.7 bar, both data sets were included in order to determine the temperature dependence of the rate constant. For two different initial concentrations of trimethylgallium, k_3 follows a single straight line in Figure 5, and the temperature-dependent rate coefficient was determined to be

$$k_3/(\mathrm{cm^3\ mol^{-1}\ s^{-1}}) = 2.34 \times 10^{11} \exp[-23330(\mathrm{K}/T)]$$

On the basis of the low A-factor from the Arrhenius plot, we can conclude that the reaction is in the fall-off region fairly close to the low-pressure limit. The pressure dependence is, however, weak.

V. RRKM Calculations

The experimental results of reaction R3 were fitted using RRKM calculations based on the variational transition state theory. Although detailed discussions of this theory are available in the literature, it is important to discuss some aspects here.

The RRKM unimolecular rate coefficient k_3^{RRKM} can be expressed as follows:

$$k_{\mathrm{uni}}^{\mathrm{RRKM}} = l^{\ddagger}\frac{k_B T}{h}\frac{Q_R^{\ddagger}}{Q_R Q_a}\exp\left(-\frac{\Delta E_0}{RT}\right)\int_0^{\infty}\frac{\sum P(E^{\ddagger})\exp(-E^{\ddagger}/RT)}{1 + k_r/\beta_c k_d[\mathrm{M}]}\,\mathrm{d}\left(\frac{E^{\ddagger}}{RT}\right)$$

$$k_r = l^{\ddagger}\frac{Q_R^{\ddagger}}{Q_R}\frac{\sum P(E^{\ddagger})}{hN(E^{\ddagger} + E_0)}$$

where $l^{\ddagger}$ is the reaction path degeneracy; k_B and h are the Boltzmann and Planck constants; Q_R, $Q_R^{\ddagger}$ are partition functions of the adiabatic rotations for the reactant and the transition state, respectively. Q is the partition function of all active modes of the reactant. E^0 is the energy barrier of the reaction at 0 K. β_c is the collision efficiency and k_d is the rate coefficient for collisional deactivation; $P(E^{\ddagger})$ is the total number of energy states of the transition state having energy $E^{\ddagger}$, and $N(E^{\ddagger} + E_0)$ is the density of energy states for the reactant having energy $E = E^{\ddagger} + E_0$. Simple bond-breaking reactions such as those depicted by R3 have so-called "loose" transition states due to the long bond length in the transition state, which is two to three times longer than the equilibrium bond length. These reactions occur barrierlessly, and the critical energy barrier equals to some extent the energy of the breaking bond. Therefore, the task was to determine the location of the transition state. This can be done by varying the reaction coordinate until the minimum of the reaction rate is reached.[40]

The calculation is based on the Gorin[40–44] model which is mainly based on four assumptions: (a) The vibrational frequencies of $GaCH_3$ (the product in reaction R3) do not change in the transition state. (b) The two external rotations with the largest moments are treated as adiabatic (they are not contributing to the thermal rate). (c) The residual external rotation and the 2 degrees of freedom representing the bending vibrations of the CH fragment in $GaCH_3$ are treated as completely free active internal rotors with moments of inertia fixed at that for an isolated CH_3 product. (d) To search the structure of the transition state, the potential energy along the reaction coordinate is modeled with a Morse potential:

$$V(r) = D_e[1 - \exp(-\beta(r - r_e))]^2$$

The Morse parameter β could be determined from the frequency representing the Ga−C stretching vibration and the energy barrier of the reaction, E_0.

This approach is widely accepted as a standard model for simple bond-fission reactions. The required geometry and frequencies of $GaCH_3$ were taken from the PBE/aug-cc-pVQT calculation. The high-pressure-limit rate coefficients, $k_3^{\mathrm{RRKM},\infty}$, were calculated as a function of the separation distance of the Ga−C bond, r_{Ga-C}, to determine the structures of the transition states.

The geometry parameters at $r_{Ga-C} = 4.8$ Å, where $k_3^{\mathrm{RRKM},\infty}$ exhibits the minimum value, were treated as the structure of the transition state for reaction R3. These findings are depicted in Figure 6. The high-pressure rate constant is normalized with

TABLE 5: Reactant and Transition-State RRKM Parameters for the Unimolecular Decomposition of $GaCH_3$

	$GaCH_3$	$Ga-CH_3^{\ddagger}$
vibrational frequencies, cm^{-1}	3009(2), 2923(1), 1376(2), 1125(1), 468(1), 458(2)[a]	3226(2), 3055(1), 1351(2), 473(1)
symmetry	C_{3v}	C_{3v}
E_0 [b]	adjusted	
σ_{sym}/n [c]	3	3
Ga−C bond length	$r_e = 2.047$ Å	$r^{\ddagger} = 4.8$ Å
Lennard-Jones parameters	$(\epsilon/k)/K = 4.92$, $\sigma/Å = 972$ [44]	

	$GaCH_3$			$Ga-CH_3^{\ddagger}$		
moments of inertia	B_{ext}/cm^{-1}	σ_i	dimension	B_{ext}/cm^{-1}	σ_i	dimension
external, inactive	0.298	1	2	0.048	1	2
external, active	6.77	3	1	9.579	3	1
internal				7.600	1	2

[a] Vibrational degeneracies are given in parentheses. [b] E_0 = critical energy. [c] σ_{sym} = symmetry number.

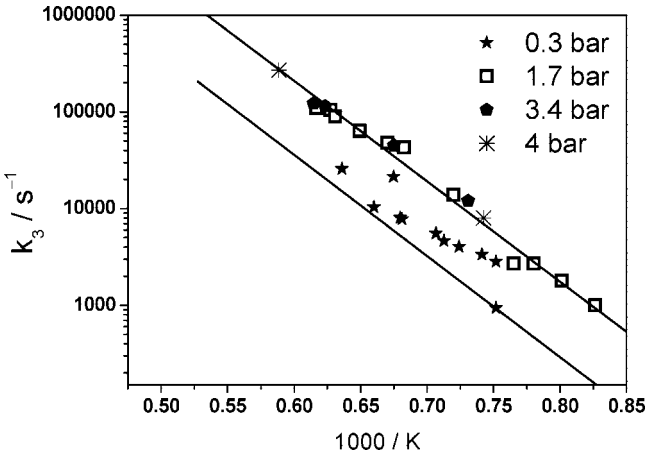

Figure 7. Arrhenius plot of the experimental rate constant k_3 at 0.3, 1.7, and 3.4 bar. The measured rates of k_3 at 1.7, 3.4, and 4 bar are similar within the experimental accuracy. All results were taken into account to extract the Arrhenius representation in Figure 5. The solid lines are the results of the RRKM calculation using the energy barrier $E_0 = 288.4$ kJ/mol and the energy transfer parameter $\langle \Delta E \rangle_{down} = 400$ cm^{-1}.

respect to the minimum high-pressure rate coefficient. Required geometries of the reactants and transition states are listed in Table 5.

The RRKM calculations were carried out using the UNIMOL suite.[40] Rate constants in the high-pressure limit were predicted by an RRKM calculation, and the pressure dependence of reaction R3 was obtained using a master-equation approach. All required input parameters for the RRKM calculations are as follows: vibrational frequencies, rotational constants for the external (B_{ext}) and internal (B_{int}) rotors, symmetry, degeneracy factors (σ), and Morse parameter β (calculated from the reaction coordinate frequency). The parameters are summarized in Table 5. Moments of inertia about the principal axis were calculated using the GEOM program from the UNIMOL suite assuming symmetric-top characteristics of the molecules. The two-dimensional internal degree of freedom representing the CH-bending vibrations is treated as free rotor. Additionally, the one-dimensional rotor along the breaking Ga−C bond is treated as active and is therefore able to exchange energy with vibrational levels. For reaction R3, the energy barrier of the reaction, E_0, which is the most sensitive parameter in the calculations, was adjusted until the RRKM rate coefficient matched our experimental data. The average downward energy transferred per collision, $\langle \Delta E \rangle_{down}$, is also unknown. This value ranges from 400 to 800 cm^{-1} for usual thermal decompositions.[46] In this calculation, the value of (400 cm^{-1}) was used. The value of $\langle \Delta E \rangle_{down}$ does not need to be estimated more precisely because E^0 is much more sensitive to the rate coefficient than to $\langle \Delta E \rangle_{down}$ and an error due to $\langle \Delta E \rangle_{down}$ is cancelled. The solid lines in Figure 7 show the RRKM results calculated with $E_0 = 288$ kJ/mol for reaction R3. The fit to our experimental data is good. Using the same energy barrier, the pressure dependence was also fairly reproduced by the RRKM calculation within the experimental errors.

VI. Conclusions

In a combined experimental and numerical effort including ab-initio calculations, the kinetics of the thermal decomposition of trimethylgallium were investigated. By analyzing the measured Ga-atom concentration profiles by means of ARAS, it was found that for temperatures between 1210 and 1630 K and pressures between 0.3 and 3.4 bar the decomposition occurs via three consecutive reactions, namely, the successive cleavage of the three Ga−C bonds. Of these, the last reaction (R3), $GaCH_3 + M \rightarrow Ga + CH_3 + M$, is the rate-determining step. The corresponding rate constant k_3—for which so far no definite information existed in the literature—was deduced by fitting the measured profiles with CHEMKIN assuming the consecutive elimination steps. The only fit parameter was the last step (R3). The required energy barriers for the other two reactions were calculated from first principles. The rate constant $k_3/(cm^3\ mol^{-1}\ s^{-1}) = 2.34 \times 10^{11} \exp[-23330(K/T)]$ corresponds to an activation energy $E_{a,3}$ of 194 kJ/mol and was found to be in the fall-off regime close to the low-pressure regime.

Additionally, the rate constants of the last step were reproduced within the framework of the RRKM theory assuming a loose transition state for the dissociation of $GaCH_3$. The energy barrier, E_3^0, was varied until the rate constant k_3 from the RRKM matched the experimental one. Required structural parameters for the RRKM calculation were obtained from the ab-initio simulations. The resulting value of 288 kJ/mol is in good agreement with the corresponding barrier computed on an ab-initio basis. Here, DFT/PBE yields essentially the same energy differences as CCSD theory. These results constitute the basis for constructing a gas-phase mechanism for material synthesis on the basis of $Ga(CH_3)_3$ decomposition.

Acknowledgment. Financial support of the German Research Foundation DFG within the SFB445 is gratefully acknowledged.

References and Notes

(1) Harwig, T.; Kellendonk, F. *J. Solid State Chem.* **1978**, *24*, 255.

(2) Dai, L.; Chen, X. L.; Zhang, X. N.; Jin, A. Z.; Zhou, T.; Hu, B. Q.; Zhang, Z. *J. Appl. Phys.* **2002**, *92*, 1062.
(3) Cheng, B.; Samulski, E. T. *J. Mater. Chem.* **2001**, *11*, 2901.
(4) Li, Y.; Trinchi, A.; Wlodarski, W.; Galatsis, K.; Kalantar-Zadeh, K. *Sens. Actuators* **2003**, *B93*, 431.
(5) Ifeacho, P.; Wiggers, H.; Schulz, C.; Schneider, L.; Bacher, G. *J. Nanopart. Res.* **2007**,
(6) Takahashi, K.; Kunz, A.; Woiki, D.; Roth, P. *J. Phys. Chem. A* **2000**, *104*, 5246.
(7) Takahashi, K.; Kunz, A.; Roth, P. *Phys. Chem. Chem. Phys.* **2001**, *3*, 4296.
(8) Herzler, J.; Roth, P. *Phys. Chem. Chem. Phys.* **2003**, *5*, 1552.
(9) Herzler, J.; Roth, P. *Phys. Chem. Chem. Phys.* **2002**, *4*, 5259.
(10) Jacko, M. G.; Price, S. J. W. *Can. J. Chem.* **1962**, *41*, 1560.
(11) DenBaars, S. P.; Maa, B. Y.; Dapkus, P. D.; Danner, A. D.; Lee, H. C. *J. Cryst. Growth* **1986**, *77*, 188.
(12) Haigh, J.; O'Brien, S. *J. Cryst. Growth* **1984**, *67*, 75.
(13) Yoshida, M.; Watanabe, H.; Uesugi, F. *J. Electrochem. Soc.* **1985**, *132*, 677.
(14) Larsen, C. A.; Buchan, N. I.; Stringfellow, G. B. *Appl. Phys. Lett.* **1988**, *52*, 480.
(15) Lee, P. W.; Omstead, T. R.; McKenna, D. R.; Jensen, K. F. *J. Cryst. Growth* **1987**, *85*, 165.
(16) Larsen, C. A.; Buchan, N. I.; Li, S. H.; Stringfellow, G. B. *J. Cryst. Growth* **1990**, *102*, 103.
(17) Oikawa, S.; Tsuda, M.; Morishita, M.; Mashita, M.; Kuniya, Y. *J. Cryst. Growth* **1988**, *91*, 471.
(18) Hase, W. L. *J. Chem. Phys.* **1972**, *57*, 730.
(19) Edwards, A. H.; Jones, K. A. *J. Chem. Phys.* **1991**, *94*, 2894.
(20) Trachtman, M.; Beebe, S.; Bock, C. W. *J. Phys. Chem.* **1995**, *99*, 15028.
(21) Maung, N. *J. Mol. Struct. (THEOCHEM)* **1998**, *432*, 129.
(22) Pelekh, A.; Carr, R. W. *J. Phys. Chem. A* **2001**, *105*, 4697.
(23) Jensen, J. O. *J. Mol. Struct. (THEOCHEM)* **2004**, *673*, 173.
(24) Schmid, R.; Basting, D. *J. Phys. Chem. A* **2005**, *109*, 2623.
(25) Timoshkin, A. Y.; Bettinger, H. F.; Schaefer, H. F. *J. Phys. Chem. A* **2001**, *105*, 3240.
(26) Moscatelli, D.; Cavallotti, C. *J. Phys. Chem. A* **2007**, *111*, 4620.
(27) Fikri, M.; Makeich, A.; Schulz, C. *Phys. Chem. Chem. Phys.*, submitted for publication.
(28) Blöchl, P. E. *Phys. Rev. B* **1994**, *50*, 17953.
(29) Kresse, G.; Furthmüller, J. *Phys. Rev. B* **1996**, *54*, 11169.
(30) Kresse, G.; Joubert, D. *Phys. Rev. B* **1999**, *59*, 1758.
(31) Perdew, J. P.; Burke, K.; Ernzerhof, M. *Phys. Rev. Lett.* **1996**, *77*, 3865.
(32) Frisch, M. J.; Trucks, G. W.; Schlegel, H. B.; Scuseria, G. E.; Robb, M. A.; Cheeseman, J. R.; Montgomery, J. A., Jr.; Vreven, T.; Kudin, K. N.; BurantJ. C.; Millam, J. M.; Iyengar, S. S.; Tomasi, J.; Barone, V.; Mennucci, B.; Cossi, M.; Scalmani, G.; Rega, N.; Petersson, G. A.; Nakatsuji, H.; Hada, M.; Ehara, M.; Toyota, K.; Fukuda, R.; Hasegawa, J.; Ishida, M.; Nakajima, T.; Honda, Y.; Kitao, O.; Nakai, H.; Klene, M.; Li, X.; Knox, J. E.; Hratchian, H. P.; Cross, J. B.; Bakken, V.; Adamo, C.; Jaramillo, J.; Gomperts, R.; Stratmann, R. E.; Yazyev, O.; Austin, A. J.; Cammi, R.; Pomelli, C.; Ochterski, J. W.; Ayala, P. Y.; Morokuma, K.; Voth, G. A.; Salvador, P.; Dannenberg, J. J.; Zakrzewski, V. G.; Dapprich, S.; Daniels, A. D.; Strain, M. C.; Farkas, O.; Malick, D. K.; Rabuck, A. D.; Raghavachari, K.; Foresman, J. B.; Ortiz, J. V.; Cui, Q.; Baboul, A. G.; Clifford, S.; Cioslowski, J.; Stefanov, B. B.; Liu, G.; Liashenko, A.; Piskorz, P.; Komaromi, I.; Martin, R. L.; Fox, D. J.; Keith, T.; Al-Laham, M. A.; Peng, C. Y.; Nanayakkara, A.; Challacombe, M.; Gill, P. M. W.; Johnson, B.; Chen, W.; Wong, M. W.; Gonzalez, C.; Pople, J. A. *Gaussian 03*, Revision C.02; Gaussian: Wallingford, CT, 2004.
(33) Becke, A. D. *J. Chem. Phys.* **1993**, *98*, 5648.
(34) Lee, C.; Yang, W.; Parr, R. G. *Phys. Rev. B* **1988**, *37*, 785.
(35) Bartlett, R. J. *J. Phys. Chem.* **1989**, *93*, 1697.
(36) Beagley, B.; Schmidling, D. G.; Steer, I. A. *J. Mol. Struct.* **1974**, *21*, 437.
(37) Kee, R. J.; Rupley, F. M.; Miller, J. A.; Coltrin, M. E.; Grcar, J. F.; Meeks, E.; Moffat, H. K.; Lutz, A. E.; Dixon-Lewis, G.; Smooke, M. D.; Warnatz, J.; Evans, G. H.; Larson, R. S.; Mitchell, R. E.; Petzold, L. R.; Reynolds, W. C.; Caracotsios, M.; Stewart, W. E.; Glarborg, P.; Wang, C.; Adigun, O. *CHEMKIN Collection*, Release 3.6; Reaction Design: San Diego, CA, 2000.
(38) Mitchell, S. A.; Hackett, P. A.; Rayner, D. M.; Cantin, M. *J. Phys. Chem.* **1986**, *90*, 6148.
(39) Lutz, A. E.; Kee, J. K.; Miller, J. A. *SENKIN: A Fortran Program for Predicting Homogeneous Gas.Phase Chemical Kinetics with Sensitivity Analysis*; Sandia National Laboratories Report SAND87-8248; Sandia Laboratories: Albquerque, NM, 1991.
(40) Gilbert, R. G.; Smith, S. C. *Theory of Unimolecular and Recombination Reactions*; Blackwell Scientific: Oxford, U.K., 1990.
(41) Smith, G. P.; Manion, J. A.; Rossi, M. J.; Rogers, A. S.; Golden, D. M. *Int. J. Chem. Phys* **1994**, *26*, 211.
(42) Benson, S. *Thermochemical Kinetics*, 2nd ed.; John Wiley and Sons: New York, 1976.
(43) Jordan, M. J. T.; Smith, S. C.; Gilbert, R. G. *J. Phys. Chem.* **1991**, *95*, 8685.
(44) Greenhill, P. G.; Gilbert, R. G. *J. Phys. Chem.* **1986**, *90*, 3104.
(45) Feron, O.; Sugiyama, M.; Nakano, Y.; Shimogaki, Y. *Electrochemical Chemical Vapor Deposition. Proceedings of the 15th International Conference on CVD*; Electrochemical Society: Pennington, NJ, 2000; p 707.
(46) Tsang, W. *Combust. Flame* **1989**, *78*, 71.

JP801516Y